Study of creep cavitation in a stainless steel weldment

Conference or Workshop Item

Study of creep cavitation in a stainless steel weldment

H Jazaeri[a], P J Bouchard[a], M Hutchings[a], P Lindner[b]
[a] Materials Engineering, The Open University, Walton Hall, Milton Keynes, MK7 6AA, UK
[b] Institut Laue-Langevin, BP 156, 38042 Grenoble Cedex 9, France

Abstract

A study of creep cavities near reheat cracking in AISI Type 316H austenitic stainless steel headers, removed from long-time high temperature operation in nuclear power plants, is reported. It is shown how application of scanning electron microscopy (SEM), cryogenic fractography and small angle neutron scattering (SANS) can be applied, in a complementary way, to observe and quantify creep cavitation damage. Creep cavities in the vicinity of the crack are found to be mainly surrounding inter-granular carbides. Trends in the size and area fraction of creep cavities relative to the crack path are quantified based on an optimised metallographic and image analysis procedure. Brittle fracture, with clear facets, of material remote from crack is achieved using a cryogenic procedure, and is compared with fractured facets of material within 8 mm of the crack which show evidence of large numbers of cavities. The SANS technique is found to be a very suitable method of quantifying creep cavitation averaged over a larger gauge volume. The distribution of cavities within the size range of 100 to 400 nm is quantified using SANS from positions normal to the crack line. It is shown that the cavity size distribution peaks at about 200 nm and this correlates closely with the quantitative SEM observations.

1 INTRODUCTION

The life-time of many engineering components operating at high temperatures is determined by time-dependent creep deformation and damage. Reheat cracking has been observed in several austenitic stainless steels and Ni-based alloys, for example see the survey of Dhooge et al[1]. A better understanding of reheat cracking creep damage development mechanisms is required in order to improve models for predicting the life-time and integrity of susceptible welded structures operating at high temperatures.

The generally accepted understanding of reheat cracking formation is that creep damage starts with nucleation of cavities which usually occurs at second phase particles in grain boundaries[2]. The nucleation process has been described as diffusion and clustering of vacancies which form cavities and is believed to be controlled by the maximum principal stress normal to the grain boundary[2]. Cavity growth[3] and linkage of coalesced cavities leads to final creep fracture. Chen and Argon[4] have shown that cavity coalescence decreases the number of cavities and creates a substantial tail in the cavity size distribution curve at very large cavity sizes. Interestingly Dyson et al. observed formation of cavities (about 200 nm size) during prior cold plastic deformation of Nimonic[5], which illustrates the potential importance of fabrication processes on damage mechanics. The kinetics of creep cavitation damage development in austenitic stainless steel is complex, depending on the material properties (e.g. creep deformation, creep ductility, thermal ageing), fabrication history (plastic strain and thermo-mechanical welding cycles), loading (residual stress, primary load, secondary load), the temperature/load history and structural effects (stress triaxiality, elastic follow-up). In order to study and understand the kinetics of reheat cracking damage development and thereby improve life-time assessment models, robust tools are required to observe and quantify creep cavitation damage.

A wide range of destructive and non-destructive techniques are available to assess creep damage based either on surface or volume analyses, as described in the recent review of Bouchard and Rist[6]. In this paper metallographic examination using scanning electron microscopy (SEM) and small angle neutron scattering (SANS) are applied to assess creep cavitation damage. Theoretically microscopic study of metallographically prepared sections using SEM allows detailed examination of creep cavities down to a few nanometres in size; however this method is highly operator dependent. The major challenge is to generate a truly representative surface by metallographic preparation. A repeated polish-etch procedure has been proposed[7-9] as a suitable preparation method for revealing cavities. However this method can enlarge cavities and therefore may be less suited for quantitative analysis of cavity sizes. SANS can provide quantitative information about creep cavitation up to about 500 nm in size, averaged over larger sample volumes. It has previously been applied to investigate reheat cracking in stainless steel[7,10]. For example SANS measurements were made on the LOQ instrument time-of-flight at the ISIS spallation neutron source with a scattering vector Q-range 0.008 to 0.1Å^{-1}, characterising cavity damage up to ~100nm (~1000 Å).

2 EXPERIMENTAL METHODS

2.1 Materials

The studies presented in this paper were carried out on slices of material from two steam headers; Header B (reference HRA 2B2/1, cast 69431) and Header C (reference HYA 1C1/1, cast 55919). Both steam headers' components had been removed after service (as recorded in Table 1) in UK Advanced Gas Cooled Reactors due to failure following the discovery of extensive reheat cracking near the header-nozzle weld, marked in Fig. 1. The headers were made of AISI Type 316H austenitic stainless steel with nominal compositions as shown in Table 1.

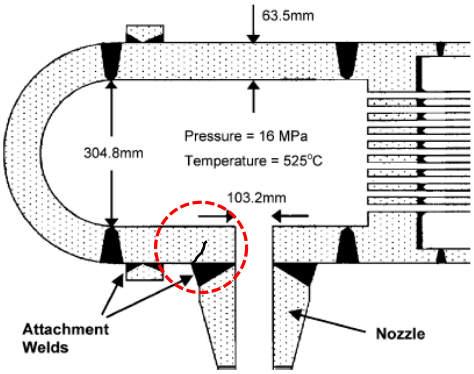

Fig. 1. Schematic diagram showing arrangement in an steam header. Sampling area near the header-nozzle weld is marked in red.

Table 1. Chemical composition and service history of the headers (remainder=Fe).

Element (wt%)	Service history Temp. (°C)/Time (Kh)	C	Mn	Si	P	S	Cr	Ni	Mo	N	Co	B
Header B	526/91	0.06	0.98	0.4	0.021	0.014	17.17	11.83	2.19	0.03	0.1	0.005
Header C	525/65	0.058	1.61	0.42	0.009	0.02	17.33	11.29	2.31	-	<0.01	

A 10 mm thick slice of material removed from steam header B was used for quantitative metallographic assessment, and a 1.2 mm thick slice from steam header C was used for SANS measurements.

2.2 Microscopic examination

Microscopic examination was carried out on 10 mm cubes extracted from slice B by electro-discharge machining (EDM). Cubes in the vicinity of the crack (1.35 mm away from the crack face), and a reference cube from a far-field region (40 mm away from the crack line) were examined. Sample preparation followed the normal metallographic procedure of sectioning,

mounting in conductive Bakelite, grinding and polishing. Grinding was carried out to 4000 μm grit size SiC papers and polishing to 0.25 μm level with diamond suspension. The final preparatory stage involved an etching procedure by immersing samples in Murakami's reagent (10g $K_3Fe(CN)_6$, 10g KOH, 100mL water) for 60 seconds. Murakami's etchant was found to be the optimum solution for sample preparation of ex-service 316H austenitic stainless steel material as it highlights grain boundary carbides without having a significant effect on the grain boundaries themselves. A Zeiss Supra 55VP FEGSEM was used to examine the sample in both Backscattered (BS) and Secondary (SE) imaging mode using an accelerating voltage of 5-10 Kv and an aperture size of 30 μm.

2.3 Cryogenic fracture

Cryogenic fracture tests were conducted on two matchstick test specimens from header B, one extracted from a far-field region and the other sampling material approaching the crack. A square sectioned matchstick of dimensions (1×1×30) mm was extracted from the far-field region and a notch at mid-length introduced to a depth of 0.4 mm by EDM in order to initiate cryogenic fracture. A larger matchstick (3×3×30) mm, was extracted from the crack mouth region with the 30 mm dimension oriented perpendicular to crack line. This matchstick was notched to a depth of 0.6 mm at 8 mm intervals along the length of specimen. The matchsticks were fixed in a specially constructed jig and soaked in liquid nitrogen (-196 °C) for approximately 5 minutes before being removed and fractured instantly.

2.4 Small Angle Neutron Scattering (SANS)

A ~1.2 mm thick slice from header C was cut with parallel faces from the 5.8 mm thick sample used in a previous SANS experiment[7]. The present SANS experiment was carried out using the D11 instrument at Institute-Laue Langevin (ILL) neutron facility in France. Details of the experiment have been reported in detail by Hutchings[11]. The D11 instrument is particularly suited to mapping material heterogeneities, such as cavities, with sizes in the range 1 to 1000 nm (10 to 10,000 Å), although to study the largest size features requires very long counting times. The incident neutron wavelength can be varied and the (1×1) m detector can be positioned inside a vacuum tank to enable scattering to be detected at a large range of scattering vectors, **Q**. The SANS intensity was measured using a circular gauge area of 5 mm diameter, corresponding to a volume of ~20 mm^3. This was centred at positions A_0, A, A_1, A_2, A_3 and E along a line perpendicular to the crack faces and located 5 mm along the crack from its mouth, at the outer surface of the header. Position A_0 was 3 mm from the crack and the other positions A_i were spaced 2 mm apart. Position E at 42 mm from the crack line was taken at the extremity of the sample as a reference position for these measurements, since cavity formation is expected to be negligible here. In this way scattering from inhomogeneities such as carbide precipitates, expected to be uniform across the sample, could be subtracted. Scattering was measured at four instrumental settings of 1.2 m, 8 m and 39 m detector distance for 6 Å incidental neutrons, and a distance of 39 m using 16.5 Å incident neutrons. In addition at each setting the transmission of each sample was measured to enable absorption corrections to be made. Scattering from a 1 mm thick water sample was measured at 1.2 m and 8 m detector distances and used to normalize the data to give absolute cross sections at these conditions. Data at 39 m were normalized by visually scaling the counts over common ranges of Q. Total counting times of ~150 min were needed for each sample position. A polydisperse distribution of spherical defect scatterers, of diameter D, was assumed in the data analysis. The most probable fractional volume distribution C(D) for cavities, where C(D)δD gives the volume fraction of cavities with diameters in the range, D to D+δD, was determined from the SANS data using a maximum entropy algorithm in the routine MAXE, developed at Southampton University and Harwell[12].

3 RESULTS

3.1 General SEM observations

The microstructure of an area in the vicinity of the crack, within 10 mm distance of the crack mouth, from header B is presented in Fig. 2. The etchant revealed carbides (I) precipitated at the grain boundaries (Fig. 2a). The grain boundaries can be traced from the inter-granular carbides as the grain boundaries themselves were barely attacked by the etchant. Fig. 2a also shows the irregular shape cavities (see location II) mostly surrounding inter-granular carbides (I) at the grain boundaries. There is also a population of much finer circular dark spots (see III in Fig. 2a) of approximately 50 nm diameter that are distributed within a ± 2 μm region along the grain boundaries. These dark spots are possibly hard precipitates associated with long-term ageing of the material. The microstructure ahead of the crack, 20-30 mm away from the crack mouth, shows the presence of grain boundary carbides (Fig. 2b). Here the carbides stand out of the microstructure with no evidence of enclosed cavities, in marked contrast to the area close to the crack where there are many carbide islands surrounded by irregular shaped cavities (e.g. dark ring II in Fig. 2a). The dark spots (III) seen close to the crack in Fig. 2a are also present on both sides of grain boundaries. Images of the far-field region (Fig. 2c) show grain boundary carbides similar to the area ahead of the crack (Fig. 2b), again with no evidence of large cavities surrounding the inter-granular carbides. Dark spots also exist in this region, possibly in lower density compared with the two other regions closer to the crack (Fig. 2a,b).

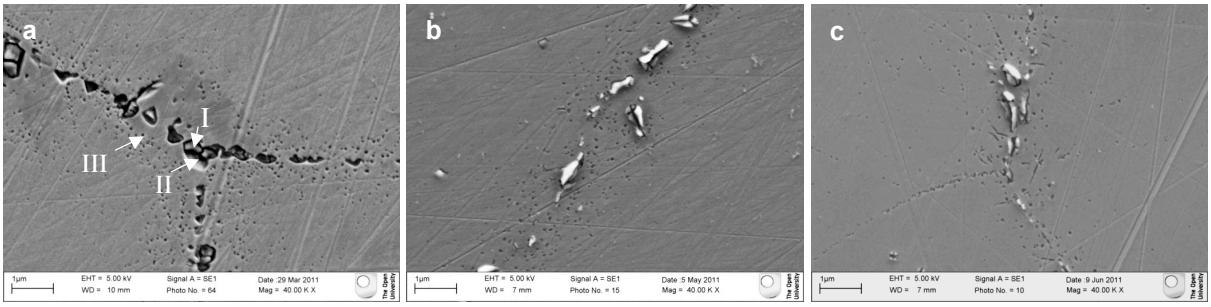

Fig. 2. a) Microstructure of an area near the crack in header B, within 10 mm of the crack mouth, showing intergranular carbides (I); many cavities (II) surrounding carbides and a population of fine dark spots adjacent the grain boundaries (III). b) Microstructure of an area along the crack, 20-30 mm away from the crack mouth, showing bright grain boundaries carbides and fine dark spots adjacent the grain boundaries. c) Microstructure of a far-field region showing bright carbides on grain boundaries with a low density of fine dark spots.

3.2 Fractography

The fracture surface of the far-field region (Fig. 3a) shows a mainly brittle fracture surface with clearly defined inter-granular facets. Fracture is mainly inter-granular with clear facets and precipitate particles at grain boundaries. A matchstick near the crack mouth was fractured at locations 8 mm, 16 mm and 24 mm away from the crack face. The fracture surfaces at 24 mm away from crack are mainly brittle in nature with clear inter-granular facets (Fig. 3b). Similar fracture surfaces are observed at 16 mm from the crack, however at 8 mm from the crack (Fig. 3c) many, but not all, of the brittle fracture inter-granular facets are cavitated.

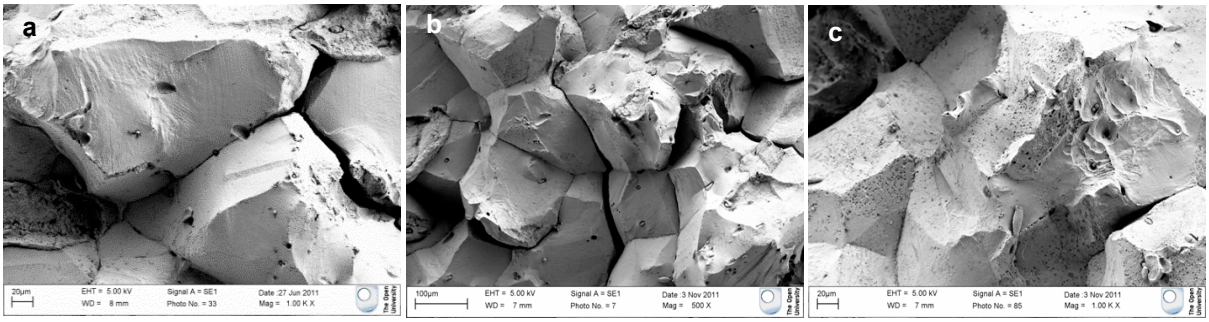

Fig. 3. Scanning electron micrographs of surfaces in header B, separated by cryogenic fracture at -196°C. a) far-field region, b) fracture surface at 24 mm away from the crack and c) fracture surface at 8mm away from the crack.

3.3 Quantitative metallography

Image analysis was undertaken in order to quantify the variation in the size and area fraction of creep cavities and precipitates, e.g. the dark spots III in Fig. 2a, in the vicinity of the crack (about 7 mm long) in Header B. For this purpose scanning electron images were acquired and analysed using ImageJ software. For quantitative analysis, BS images were chosen in preference to secondary electron images. BS images are produced mainly due to atomic number contrast making it easier to discriminate between carbides and cavities. Images were acquired at an accelerating voltage of 10Kv and magnification of 20K times. Such a large magnification was selected to have sub-micron inter-granular cavities and other features in the field of view. Sequential images were acquired at different positions normal to the crack and also along the crack line. By defining an appropriate threshold it was possible to separate creep cavities and precipitates, e.g. III in Fig. 2a, which appeared darker against the background, from neighbouring bright carbides (e.g. I in Fig. 2a). At each position a series of images were analysed sampling on average over 1500 cavities and precipitates. Edge features were excluded from the analysis and cavities up to area size of 0.8 μm^2 measured (about a micron diameter circular). Cavities and precipitates were discriminated according to their shape difference using a circularity factor = $4\pi(\text{area})/(\text{perimeter})^2$; equal to 1.0 for a perfect circle. Non-circular cavities and circular precipitates features were separated using a circularity factor of 0-0.5 and 0.5–1.0, respectively. The results are shown in Fig. 4.

The analysis of the far-field sample (Fig. 2c) showed that the average inter-granular carbide size was 100 nm diameter (cross sectional area of 0.0078μm^2) with an area fraction of 0.15%.

Quantitative analyses of the cavities and precipitates (dark spots) were carried for sampling locations along a line normal to the crack at a depth of 6 mm from the crack mouth. The variations in feature size (cross sectional area in μm^2) and area fraction of cavities as a function of normal distance from the crack face are presented in Fig. 4a. There is no significant trend in these metrics moving up to 7 mm away from the crack face, but the entire parameters drop at 9 mm.

The area fraction and size of cavities as a function of distance from the crack mouth (2.5, 4, 6, 8 and 9 mm) along a line 1.5 mm adjacent to the crack face is presented in Fig. 4b. Data related to non-circular cavities show that the size and fraction of cavities rise approaching the mouth of the crack. However there is a more rapid increase in the area fraction compared to the size of these cavities which suggests an increase in number of cavities approaching to the crack mouth.

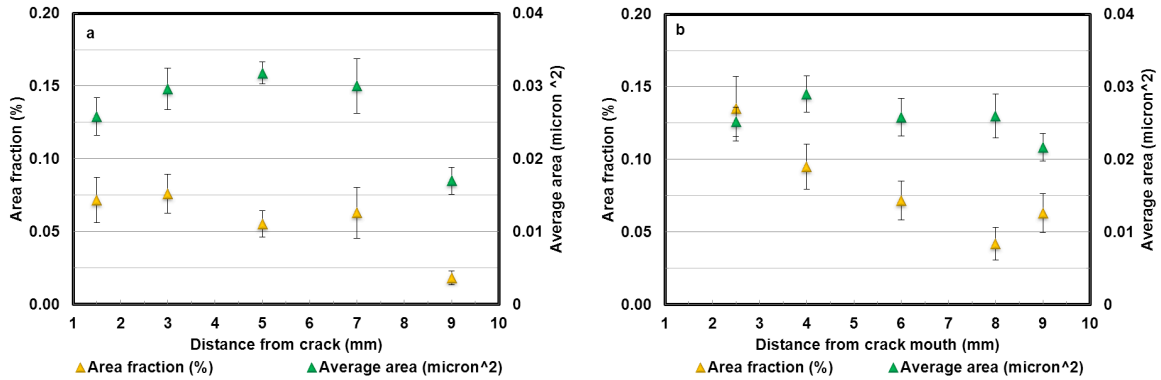

Fig. 4. Variation in the size and area fraction of cavities in header B (non-circular features using circularity factor of 0-0.5); a) as a function of distance from the crack face, at a depth of 6 mm from the crack mouth and b) as a function of distance from the crack mouth.

3.4 SANS results

The fractional size distribution of cavities C(D) for different positions moving perpendicularly away from the crack in header C is presented in Fig. 5. This has been calculated by subtracting the relative distribution of defects in position E from that for the other positions (A_i). Fig. 5 shows the increase in fractional size distribution of cavities approaching the crack. It is seen that the main cavity size lies between 500 Å and 5000 Å, peaking in the region 1000 Å to 3000 Å (1 Å = 0.1 nm).

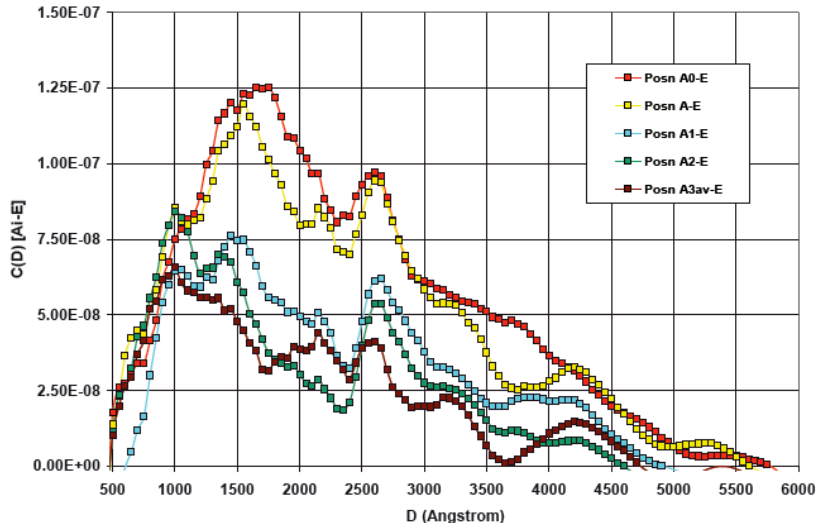

Fig. 5. The increase in true fractional size distribution (C(D)) of cavities approaching the crack in header C.

At all positions measured there is a distribution of smaller defects in the region 150 Å to 500 Å peaking at about 300 Å. This is independent of position and is consistent with the finer dark spots seen by SEM reported in section 3.1.

4 DISCUSSION

Microscopic examinations have revealed the presence of creep cavities in the vicinity of the crack from header B. The cavities appear as dark/irregular regions surrounding bright inter-granular carbides in the microscopic observations (e.g. see Fig. 2a). Samuels et al.[8] similarly reported the presence of dark rings 50-100 nm wide surrounding grain boundary carbides in an ex-service Cr-Mo ferritic steel. Fractography of material near to the crack revealed a large number of creep cavities on the inter-granular fracture surfaces (Fig. 3c) near to the crack (8 mm from crack line). Quantitative analysis of cavities along a line normal to the crack also showed an increase in size and area fraction of cavities approaching the crack (7 mm away the

crack, see Fig. 4a). Study of the cavities along the crack revealed (Fig. 4b) a more rapid increase in the area fraction of non-circular cavities compared with the size of cavities approaching the crack mouth. This suggests that the increase in area fraction is a combination of an increase in cavity size as well as a larger number of cavities, as it has been reported previously[7]. The average cavity area in the vicinity of the crack (see Fig. 4a) lies in the range 0.017- 0.03 μm^2 (that is 150 to 200 nm diameter in size). This is in good agreement with the SANS data acquired in this study where cavities in the order of 1000 to 4000 Å (100 to 400 nm) and peaking about 2000 Å (200 nm) were measured (Fig. 5). Previous quantitative metallography of a similar reheat crack[7] indicated an average cavity area of 0.2-0.25 μm^2 (500-560 nm diameter in size) within 10 mm vicinity of the crack. This is larger than measured in the current study, albeit on a different header. The previous work quantified cavity sizes by examining images acquired at lower magnification of 2,000×, compared with a magnification of 20,000× used here. Although study at lower magnification provided an overview of microstructure with good visibility of mainly large cavities, accurate measurement of sub-micron cavities may well have been compromised. Here a larger magnification was specifically used in order to quantify inter-granular sub-micron cavities (area < 0.8 μm^2) more accurately.

5 CONCLUSIONS

This study shows how application of microscopy, fractography and SANS techniques can be used, in a complementary way, to observe and quantify creep cavitation damage in the vicinity of a reheat crack in an ex-service stainless steel component. An optimised metallographic preparation technique has been developed and applied for detailed SEM studies that have revealed cavities to be mainly surrounding inter-granular carbides. The trends in the size and area fraction of these creep cavities relative to the crack path have been found. Brittle fracture with clear facets of far-field (remote from crack) material has been achieved using a cryogenic procedure, and evidence of large numbers of cavities observed on brittle fracture surfaces within 8 mm of the crack. SANS measurements have been successfully undertaken and the distribution of cavities within the size range of 100 to 400 nm quantified as a function of distance normal to the crack line. The cavity size distribution peaks at about 200 nm which correlates closely with the quantitative SEM observations.

ACKNOWLEDGEMENTS

Funding for the research from EDF Energy is gratefully acknowledged.

REFERENCES

1 Dhooge, A. Survey on reheat cracking in austenitic stainless steels and Ni base alloys. *Welding in the World* **41**, 206-219 (1998).

2 Riedel, H. Cavity nucleation at particles on sliding grain boundaries. A shear crack model for grain boundary sliding in creeping polycrystals. *Acta Metallurgica* **32**, 313-321 (1984).

3 Hales, R. The role of cavity growth mechanisms in determining creep-rupture under multiaxial stresses. *Fatigue & Fracture of Engineering Materials & Structures* **17**, 579-591 (1994).

4 Chen, I. W. & Argon, A. S. Creep cavitation in 304 stainless steel. *Acta Metallurgica* **29**, 1321-1333 (1981).

5 Dyson, B. Constraints on diffusional cavity growth rates. *Metal Science* **10**, 349 (1976).
6 Bouchard, P. J. & Rist, M. A. Creep damage measurement methods review. (The Open University, OU/MatsEng/003, 2010).
7 Bouchard, P. J., Withers, P. J., McDonald, S. A. & Heenan, R. K. Quantification of creep cavitation damage around a crack in a stainless steel pressure vessel. *Acta Materialia* **52**, 23-34 (2004).
8 Samuels, L. E., Coade, R. W. & Mann, S. D. Precracking structures in a creep-ruptured low-carbon Cr-Mo steel: Their nature and detection by light microscopy and scanning electron microscopy. *Materials Characterization* **29**, 343-363 (1992).
9 Ueno, F., Aoto, K. & Wada, Y. Study on metallographic damage parameter in creep-damage-dominant condition under creep-fatigue loading. *Nuclear Engineering and Design* **162**, 85-95 (1996).
10 Bouchard, P. J., Fiori, F. & Treimer, W. Characterisation of creep cavitation damage in a stainless steel pressure vessel using small angle neutron scattering. *Applied Physics A: Materials Science and Processing* **74**, S1689-S1691 (2002).
11 Hutchings, M. T. The use of small angle neutron scattering for mapping creep cavitation damage in an ex-service steam header. (The Open University OU/MatsEng/025, 2012).
12 Potton, J. A., Daniell, G. J. & Rainford, B. D. A new method for the determination of particle size distribution from Small-Angle Neutron Scattering Measurements. *J. Appl. Cryst* **21**, 891-897 (1988).